

Use of Laser Scanning Confocal Microscopy for Characterizing Changes in Film Thickness and Local Surface Morphology of UV-Exposed Polymer Coatings

Li-Piin Sung, Joan Jasmin, Xiaohong Gu, Tinh Nguyen, and Jonathan W. Martin—
National Institute of Standards and Technology*

Laser scanning confocal microscopy (LSCM) has been used to characterize the changes in film thickness and local surface morphology of polymer coatings during the UV degradation process. With the noninvasive feature of LSCM, one can obtain thickness information directly and nondestructively at various exposure times without destroying the specimens or deriving the thickness values from IR measurement by assuming uniform film ablation. Two acrylic polymer coatings were chosen for the study, and the physical and chemical changes of the two systems at various exposure times were measured and analyzed. Those measurable physical changes caused by UV exposure include film ablation, formation of pits and other surface defects, and increases in surface roughness. It was found in both coatings that changes in measured film thickness by LSCM were not correlated linearly to the predicted thickness loss using the changes in the CH band obtained by the Fourier Transform Infrared (FTIR) spectroscopy measurements in the later degradation stages. This result suggested it was not a uniform film ablation process during the UV degradation. At later stages, where surface deformation became severe, surface roughness and profile information using LSCM were also proven to be useful for analyzing the surface degradation process.

Keywords: Atomic force microscopy, FTIR, laser scanning confocal microscopy, photodegradation, durability, physical properties, weatherability, surface roughness, surface morphology

Understanding the mechanism and progress of UV degradation is one of the keys for predicting the service life of polymeric coatings. To achieve this objective, extensive research efforts¹⁻⁶ both in outdoor- and indoor-accelerated weathering exposures have been carried out to investigate the influences of various climatic parameters on coating degradation, and to further establish the correlation between physical and chemical degradation. Typically, appearance-related measurements, such as gloss retention and color fading, are used to assess physical degradation and define the failure of the weathered coatings. Spectroscopic measurements, such as Fourier transform infrared (FTIR) spectroscopy, are often used for monitoring chemical degradation occurring in an exposed coating. Most studies³⁻⁶ have focused on identifying primary chemical changes and assessing the rates of degradation under specific exposure conditions. The results have provided some understanding about the initial chemical degradation mechanism in the coatings.

However, the link between specific chemical and physical changes (for example, gloss loss) in a coating has re-

mained elusive, and inconsistent results as shown by investigators have been reported for various coatings and exposure conditions (both in outdoor- and indoor-accelerated weathering tests).^{2,7} Consequently, the lack of correlation between gloss loss and chemical changes measured by spectroscopy has severely limited the ability to measure and predict service life accurately. Obviously, the difficulty in comparing FTIR results with gloss measurements is that no direct link has been established between the two measurements. The FTIR measures the concentration of chemical species in coating structures while the gloss measurement "sees" the surface morphology of a coating. To make reliable comparisons between the FTIR results and gloss measurements, the correlation between surface morphology and chemical changes must be investigated concurrently. Many attempts⁸⁻¹¹ have been made to link surface morphology with gloss measurements and/or chemical changes. For example, using atomic force microscopy (AFM), VanLandingham et al.¹¹ have attempted to relate the formation of pits and surface roughening of acrylic melamine coatings to hydrolysis in the early stages of ex-

Presented at the 81st Annual Meeting of the Federation of Societies for Coatings Technology, November 13-14, 2004 in Philadelphia, PA.
*Polymeric Materials Group, Building and Fire Research Laboratory, Gaithersburg, MD 20899-8615.

posures. In this case, no observable change in film thickness was detected. However, for later stages of degradation, the change in film thickness is also an important physical parameter for comparing against the chemical changes measured by FTIR.

AFM is a useful tool for characterizing nanoscale surface deformation in the early stages of physical degradation. However, with the maximum scanning area being limited to $100 \times 100 \mu\text{m}$, and the maximum measurable peak-to-valley height being less than $6 \mu\text{m}$, AFM is not suitable for measuring the film thickness and surface morphology changes in the entire range of degradation. Destructive methods such as scanning electron microscopy (SEM) are often used to measure the final surface degradation and thickness of a film, but it is not a practical method for monitoring changes in the same sample after different exposure times. Other sensitive surface roughness and profile techniques, in the contact mode typically, have been used to characterize surface roughness and morphology. This type of instrument, such as stylus surface profiler, provides very precise surface roughness measurements, but might disturb the surface structure (especially for a fragile, degraded surface with cracks and pits) and introduce artifacts during the measurements. Thus, a nondestructive, noninvasive tool such as interference microscopy or confocal microscopy is more suitable to monitor physical changes throughout the entire degradation process. Additionally, recent efforts at NIST¹²⁻¹⁴ linking the surface morphology and subsurface microstructure to the optical reflectance properties of a coated material using a ray scattering model have provided an approach to calculate and understand the optical reflectance (related to gloss values) for a given surface morphology/microstructure. By correlating the time evolution of the physical changes, such as thickness and surface deformation (pits and cracks), to the chemical changes of a UV-exposed coating, we can quantify the process and un-

derstand the mechanism of degradation. With the methodology developed for modeling the optical reflectance from a given surface morphology or microstructure, we might be able to establish a “direct” correlation between failure assessment evaluated by gloss loss and chemical changes measured by spectroscopy.

In this research, the physical and chemical degradation of two UV-exposed coating systems—acrylic-urethane (AU) and acrylic-melamine (AM)—were studied. Physical changes caused by UV exposure, including film ablation, formation of pits, and other surface defects, were characterized by laser scanning confocal microscope (LSCM). The film thickness measured using LSCM was compared to the predicted film thickness obtained from changes in the CH band absorbance by FTIR measurement, assuming uniform film ablation for both systems. Time evolution of surface morphology of UV-exposed coatings will be presented and related to FTIR chemical changes.

EXPERIMENTAL*

Materials and Sample Preparation

Two thermoset coating systems, acrylic-urethane (AU) and acrylic-melamine (AM), were used in this study. The acrylic-urethane coating consists of a mixture of hydroxy-terminated acrylic resin (PPG lot # 00123-19, a mixture of 70.2% acrylic polymer and 29.8% 2-heptanone) and an aliphatic isocyanate crosslinking agent (Desmondur N3200). The solid content ratio of acrylic resin to iso-

*Certain instruments or materials are identified in this paper in order to adequately specify experimental details. In no case does it imply endorsement by NIST or imply that it is necessarily the best product for the experimental procedure.

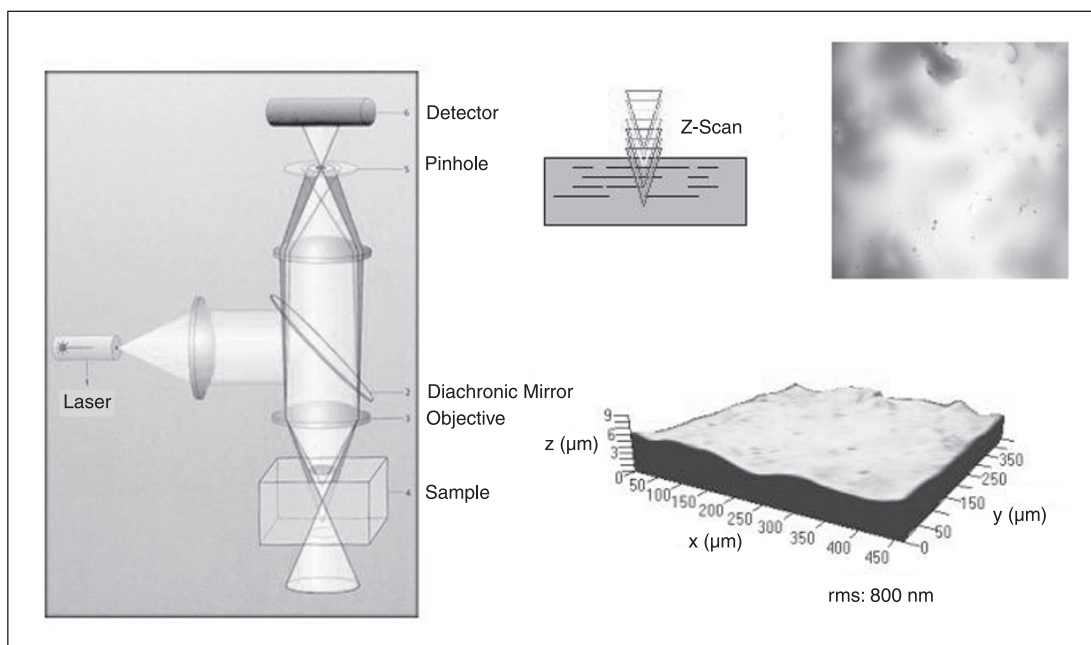


Figure 1—Schematics of an LSCM optical system and typical results in 2D intensity projection and 3D topography presentations.

cyanate crosslinking agent was 65:35. All percentages and proportions are expressed as mass fraction. To achieve a uniform film thickness of 10 μm or less by spin coating, the mixture was diluted in toluene to a final concentration of 60% acrylic-urethane. After degassing, the solution was spin-casted onto a 101.6-mm diameter silicon substrate (double-sided polished silicon wafer) at 2000 rpm for 120 sec. The coating films were then cured at 130°C for two hours. After the films were cured, the 101.6-mm diameter sample was cut into 12 specimens of 17-mm sized squares, which were suitable for UV exposure. Nine replicates were chosen and exposed under UV light. The physical and chemical changes due to UV degradation were monitored and characterized every week using AFM on three replicates, and using both LSCM and FTIR on the other six replicates. Three unexposed samples were used for the thickness measurements using SEM and interference microscopy techniques.

The acrylic-melamine coating films were prepared, cured, and conditioned using the same procedure. The acrylic-melamine coating consisted of a hydroxy-terminated acrylic resin (PPG lot# 00123-19) and a partially methylated melamine resin (Cytex industries Cymel 325). The solid content ratio of acrylic resin to melamine resin was 70:30.

UV Exposure Experiments

The UV exposure experiments were conducted using a solar simulator from Oriol Instruments. The instrumentation of the UV exposure system has been described elsewhere.^{4,5} The UV exposure conditions used in this study were full UV light (approximately 1.3 sun) and $75 \pm 3\%$ relative humidity (RH) at $50^\circ \pm 0.5^\circ\text{C}$. The light source is equipped with a 1000 W xenon arc lamp, and the wavelength ranged from approximately 270 nm to approximately 800 nm.

Fourier Transform Infrared Spectroscopy

Coating degradation was followed by FTIR spectroscopy in the transmission mode using an autosampling accessory. At each specified time, coated silicon plates were removed from the exposure cell and fitted into a demountable 150-mm diameter ring of the autosampling device. The ring was computer-controlled and could be rotated and translated to cover the entire sampling area. Spring-loaded Delrin clips ensured that the specimens were precisely located and correctly registered. Detailed design of this autosampling system has been described elsewhere.⁵ Since the exposure cell was mounted precisely in the autosampler, error due to variation of sampling at different exposure times was essentially eliminated. The spectrometer compartment was equipped with a liquid nitrogen-cooled

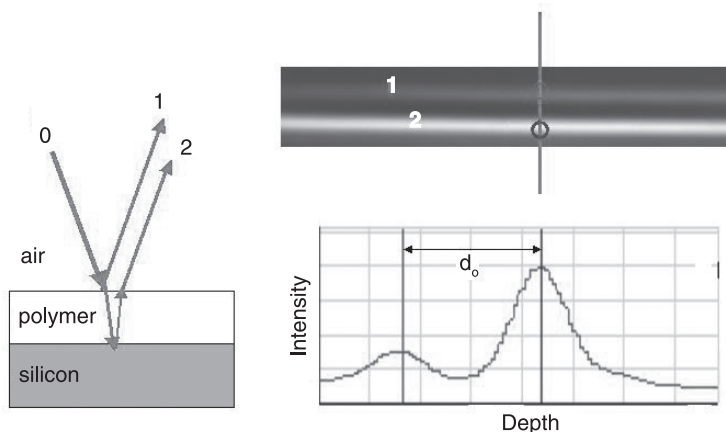


Figure 2—Illustration of the principle used for determining film thickness using LSCM line scans.

mercury cadmium telluride (MCT) detector. Spectra were recorded at a resolution of 4 cm^{-1} using dry air as the purge gas. All spectra were the average of 132 scans.

Atomic Force Microscopy

A Dimension 3100 Scanning Probe Microscope from Digital Instruments was operated in tapping mode to characterize the surface morphology of coating films before and after UV exposure. Commercial silicon microcantilever probes were used. Topographic and phase images were obtained simultaneously using a resonance frequency of approximately 300 kHz for the probe oscillation and a free-oscillation amplitude of $62 \pm 2\text{ nm}$. The set-point ratio (the ratio of set point amplitude to the free amplitude) ranged from 0.60–0.80.

Laser Scanning Confocal Microscopy

A Zeiss model LSM510 reflection laser scanning confocal microscope was employed to measure the film thick-

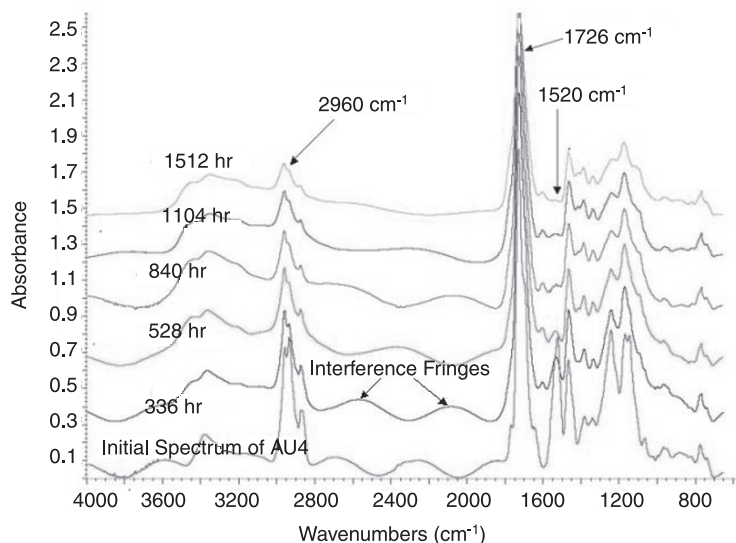


Figure 3—FTIR spectra of an acrylic-urethane (AU) coating at various UV exposure times.

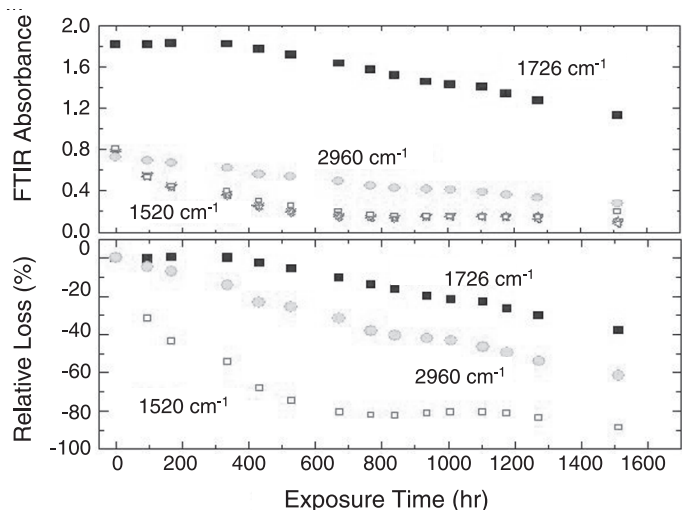


Figure 4—Upper graph shows three selected FTIR absorbance peaks of AU coatings as a function of UV exposure time; the bottom graph presents the relative changes for each peak. Uncertainty of data is estimated to be 2% ($k = 2$), the size of the error bar is smaller than the symbols.

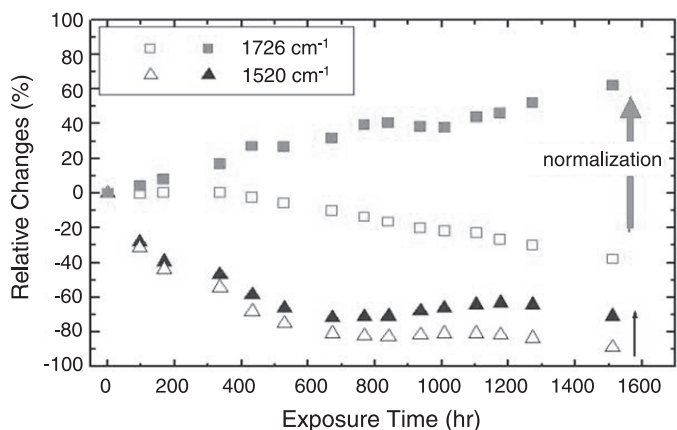


Figure 5—Relative changes of the C=O band (1726 cm^{-1}) and chain scission (1520 cm^{-1}) with (solid symbols) and without (open symbols) normalized by the CH band at the same exposure time. The arrows indicate the direction of changes after taking into account the changes in the CH band. Uncertainty of data is estimated to be 2% ($k = 2$), the size of the error bar is smaller than the symbols.

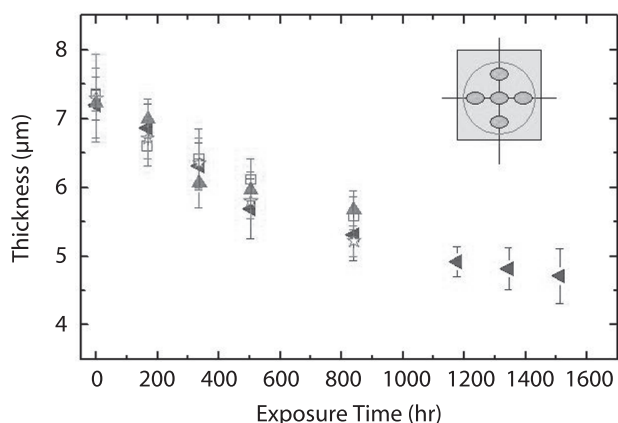


Figure 6—Film thickness obtained from six replicates of AU coatings measured using LSCM as a function of UV exposure time. The insert graph illustrates five different scanning locations on each sample.

ness and characterize the surface morphology (topographic profile) of the coatings at various UV exposure times. As illustrated in *Figure 1*, LSCM utilizes coherent light and collects light exclusively from a single plane (a pinhole sits conjugated to the focal plane) and rejects light out of the focal plane. The wavelength, numerical aperture (N.A.) of the objective, and the size of the pinhole dictate the resolution in the thickness or axial direction.¹⁵ By moving the focal plane, single images (optical slices) can be combined to build up a three-dimensional stack of images that can be digitally processed.

Unlike AFM, the measured surface area of LSCM can be as large as $2.6 \times 2.6\text{ mm}$ down to $20 \times 20\text{ }\mu\text{m}$ by using different objectives of the instrument. LSCM is not a small foot print measurement instrument, but an instrument with measurement capability covering a wide range of length scales. In this article, we focused on reporting a nondestructive metrology for thickness measurements and monitoring local changes in surface roughness/morphology to investigate the UV degradation of polymeric coatings. LSCM images presented in this article were in 2D intensity projection or 3D topographic profile and they were representative of a series of overlapping optical slices (a stack of z-scan images) with each z-step measuring $0.1\text{ }\mu\text{m}$. Without specification, each frame consisted either of 512×512 pixels or $184 \times 184\text{ }\mu\text{m}$ in size. The laser wavelength used was 543 nm .

In addition to a typical frame-scanning mode to generate a topographic profile of the coatings, LSCM was used in the line-scanning mode to measure a cross-section profile through a clearcoating, as shown in *Figure 2*. As the first principle of ray reflection, ray 1 was reflected from the air-polymer interface, and ray 2 was reflected from the polymer-silicon interface, as illustrated in *Figure 2*. For normal incident condition and assuming no light absorption in the coatings, the reflected intensity of ray 1 and ray 2 can be expressed as follows:

$$I_{Ray1} = I_o \left(\frac{n_p - n_o}{n_p + n_o} \right)^2 ; I_{Ray2} = I_o \left(\frac{4n_p \times n_o}{(n_p + n_o)^2} \right)^2 \left(\frac{n_p - n_{si}}{n_p + n_{si}} \right)^2$$

Here, I_o is the incident intensity and n_o , n_p , and n_{si} are the indices of refraction for air, polymer coatings, and silicon substrate. Strictly, one can deduce the value of n_p by calculating the relative intensity of I_{Ray1}/I_{Ray2} using the values of $n_o = 1$ and $n_{si} = 4.05$ at laser wavelength 543 nm . Then the coating thickness d_p is equal to $n_p \times d_o$, where d_o is the distance between two interfaces measured by LSCM, assuming traveling through a medium of refractive index of 1. To demonstrate that the thickness obtained from LSCM was as accurate as from other traditional thickness measurement methods, we compared thickness measurements obtained from LSCM on a fresh AM coating to results measured by SEM and interference microscopy (IM). The results were: $d = (4.43 \pm 0.47)\text{ }\mu\text{m}$ by LSCM; $d = (4.45$

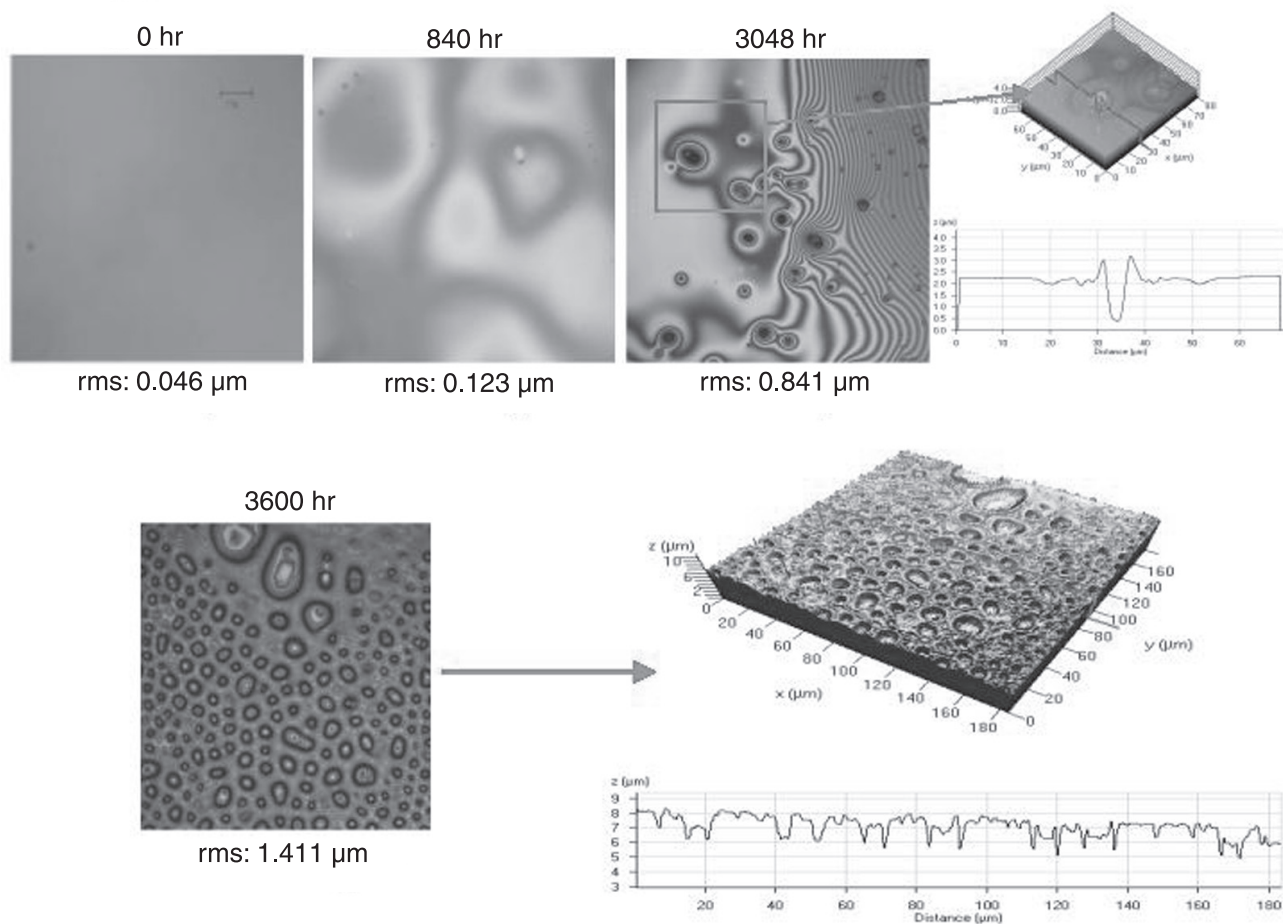


Figure 7—LSCM images (2D intensity projection) of AU film for four different exposure times. The corresponding topographic images and height information are also presented. Each LSCM micrograph consists of 512 x 512 pixels and 184 x 184 μm by size.

± 0.23 μm by IM; and $d = (4.40 \pm 0.15)$ μm by SEM. All thickness results were averaged from three to five locations from the same specimen at similar locations and the results from the three techniques (LSCM, SEM, IM) were consistent.

RESULTS AND DISCUSSION

Chemical Changes in UV-Exposed Acrylic-Urethane Coatings

FTIR spectra of AU coatings before and after UV exposure to different times are shown in Figure 3. The low intensity interference fringes in the spectra are often used to determine the film thickness using the interval between the fringes.⁶ However, as film thickness decreased and the surface became rougher, the peak intensity and phase of interference fringes changed as well as the width of the peak (as shown in Figure 3). It then became problematic to determine the film thickness using the interference fringes. Thus, laser scanning confocal microscopy was used to determine the film thickness at any

given exposure time, and the results are presented later.

Here, we focus only on the time-evolution of three selected FTIR peaks related to the CH stretching band at 2960 cm^{-1} (mass loss), NH bending and CN stretching at 1520 cm^{-1} (chain scission), and the C=O band at 1726 cm^{-1} in the AU coatings. Clearly, the peak intensity (FTIR absorbance at peak maximum) of these bands decreased as exposure time increased (as shown in Figure 4). The relative loss of each peak, with respect to the initial absorbance at zero exposure time, is also plotted in the bottom graph. The 2960 cm^{-1} CH band lost about 4% in intensity per hour; and the chain scission peak at 1520 cm^{-1} decreased rapidly with only 20% left by 600 hr, reaching a constant level (80% loss) afterward. Chemical changes are often presented as the relative rate of appearance or disappearance of a given FTIR band by normalizing to the CH band, on the assumption that the CH band is a measure of the amount of materials that remains. The mass change is assumed to be directly related to film thickness changes (the linear reduction in the coating thickness, i.e., film ablation), as several researchers have indicated in their reports.^{3,6} Accordingly, this assumption implies that degradation is an ablation process taking place in a

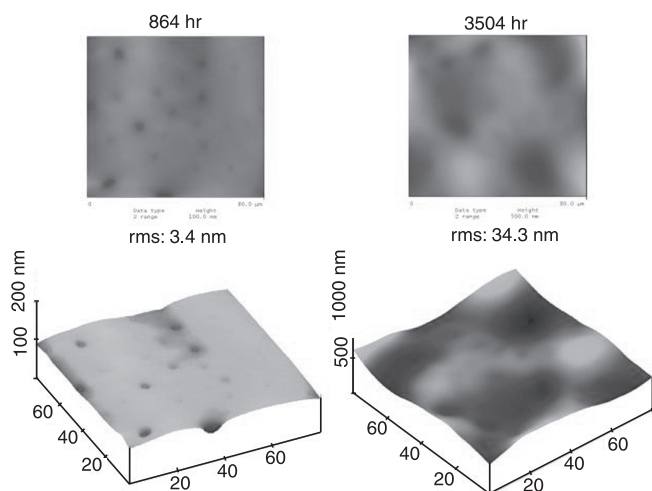
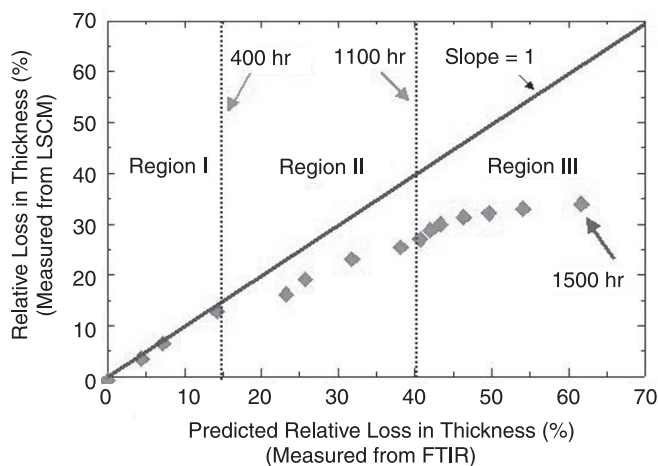
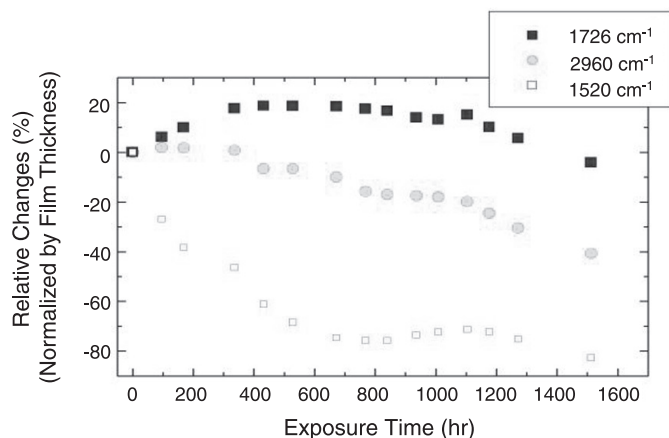


Figure 8—AFM images of the AU coatings at two different exposure times.

Figure 9—Comparison of the relative loss between the predicted values from the FTIR peak at 2960 cm^{-1} and the measured values using LSCM. Uncertainty of data is estimated to be 7% ($k = 2$).Figure 10—Relative changes in C=O band (1726 cm^{-1}), CH band (2960 cm^{-1}), and chain scission (1520 cm^{-1}) normalized by the film thickness at the same exposure time. Uncertainty of data is estimated to be 2% ($k = 2$), the size of the error bar is smaller than the symbols.

steady manner from an outer layer that remains consistent through the exposure period.

Figure 5 compares the relative changes for the chain scission peak at 1520 cm^{-1} and loss of the C=O band at 1726 cm^{-1} with (solid symbols) and without (open symbols) normalized to the changes in the CH band. It is clear that without taking into account the mass loss (changes in CH band) in the process of the UV degradation the rate of chain scission is faster than that normalized by the CH band. On the other hand, for those FTIR peaks (such as the C=O band in Figure 5) decaying slower than the corresponding CH band, a decay curve of C=O would be replaced by an increasing or growing profile after taking into account the normalization by the CH band. The results are conflicting and depend on the chosen normalizing factor. Thus, it is difficult to compare these results and understand degradation of these chemical changes. The real issue is to select a reference IR band which has a well-known characteristic property or remains constant in the UV degradation process. One approach, as suggested by Croll et al.⁶ is to use the film thickness, assuming film ablation occurred, as a normalized factor for analyzing chemical changes. However, in this approach, the thickness of the coatings and the surface morphology should be examined carefully to relate the chemical changes obtained from FTIR measurements to thickness and surface morphology measurements to understand the degradation mechanism.

Thickness and Surface Morphology Changes of UV-Exposed AU Coatings

For comparison with FTIR results, we conducted the microscopy measurements at five different scanning locations on a sample with each scan location being at least 2 mm apart, as illustrated in the insert graph of Figure 6. These five locations were fixed locations chosen from zero exposure time and measured at all exposure times prior to when surface deformation dominated. At each location, the surface morphology was also characterized. At each scanning location (scan length $\sim 184\text{ }\mu\text{m}$), 10 different thickness values were extracted. Thus, each data point in Figure 6 is the average value of as many as 50 different locations. The error bar represents the range of $k = 2$ uncertainty (at 95% confidence level). All samples followed the same trend. The film thickness decreased linearly (about 3 nm/hr) in the early stages of degradation then slowly decreased to a constant value after 1100 hr of UV exposure. The sample lost only 35% of its original thickness after 1500 hr of exposure

compared to a 63% loss as estimated using the CH band in FTIR measurement. This large discrepancy can be explained as follows: in the late stage (after 1100 hr), the surface became rough, and the thickness values obtained were only from limited filled areas that excluded pits and other surface deformations. However, the coatings maintained the same thickness but with an increasing area of pits and holes on the surfaces. Although the thickness value was only measured from the filled areas, we have estimated the areas of pits and holes were less than 5% of the total measured area at 840 hr exposure time and up to about 20% at 1500 hr; and most of the pits and holes were shallow. Therefore, the filled areas are still the representative majority and the thickness value is not far from the “true or average” thickness value. We concluded that there is an unaccountable discrepancy between the losses in “average” thickness to that in CH band.

Surface morphological changes were analyzed at various exposure times using LSCM and AFM. The changes in surface morphology and pit/hole formation are clearly demonstrated in *Figures 7* and *8*. The surface roughness data were provided in the figures for reference. Initially, the surface appeared to be smooth and featureless. As the exposure time increased, surface roughness increased and the appearance of pits/holes was observed. For example, the root-mean-square (rms) roughness value of the coating surface at 3,504 exposure hours was ten times larger than the rms surface roughness value at 864 exposure hours, as shown in *Figure 8*. The size of pits increased further and merged with other nearby pits. In the later stages, the film appeared to be very rough with pronounced surface patterns as a result of degradation. These local physical changes contribute mass changes and might be related to other degradation processes. More analyses are underway to calculate surface roughness and relate to the results obtained from gloss measurements.

Correlation between Chemical and Physical Changes of UV-Exposed AU Coatings

After observing how the thickness and surface features changed in the UV degradation of the AU coating, the assumption does not seem to be correct that degradation and film ablation occurred in a steady manner from an outer layer that remains consistent through the exposure period. Thus, using a CH band as a normalizing factor for analyzing chemical changes in the UV degradation process might not be accurate. To evaluate the validity of using the film thickness as a normalizing parameter for analyzing FTIR spectra, we first compared the relative loss in the actual

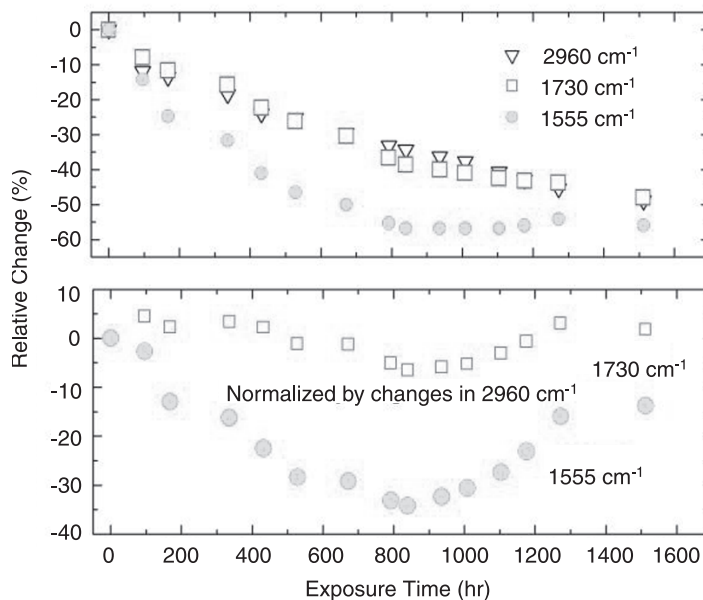


Figure 11—Upper graph: relative changes in FTIR absorbance peak at 2960, 1730, and 1555 cm^{-1} as a function of UV exposure time for six AM coatings. Bottom graph: relative changes of 1730 cm^{-1} , and 1555 cm^{-1} band normalized by 2960 cm^{-1} band. Each data point is an average of six replicates, and the error bar is smaller than the symbols.

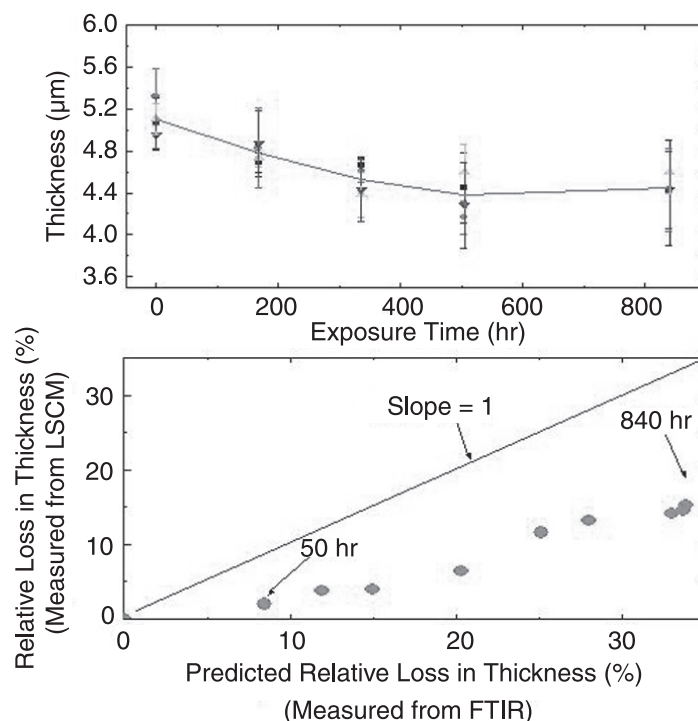


Figure 12—Upper graph: the measured film thickness of six AM coatings as a function of exposure time. The line is the averaged values of six samples; bottom graph: comparison between the predicted relative loss in thickness from FTIR peak at 2960 cm^{-1} and the relative loss in film thickness measured by LSCM. The estimated uncertainty of data in the bottom graph is about 10%, mostly due to the uncertainty in the film thickness measurement, especially in the late stages.

“measured” film thickness using LSCM to the “predicted” film thickness assuming mass loss (CH band at 2960 cm^{-1}) due to uniform film ablation.

As shown in *Figure 9*, the relationship between relative loss in the “measured” and “predicted” film thickness followed the linear relationship (slope = 1) for the initial state (region I), then deviated from the linear relationship after 400 hr of exposure time. In conjunction with the observation of surface morphology changes, we cataloged the degradation process into three regions:

REGION I ($t \leq 400\text{ HR}$): the physical change was due to uniform film ablation; the mass loss was proportional to the loss in film thickness; no significant changes in surface morphology (pits were small and were not observed in the LSCM measurement). In this region, no changes in gloss would be expected.

REGION II ($400\text{ HR} \leq t \leq 1100\text{ HR}$): film thickness continued to decrease; pits started to form and grow (see AFM images), and the coating surface became rougher as exposure time increased. Gloss loss should be expected in this region due to the surface roughening and pit formation.

REGION III ($1100\text{ HR} \leq t \leq 1500\text{ HR}$): the later stages of the physical degradation—pits merged with nearby pits/cracks, larger patterns formed, and surface roughness continued to increase. In this region, the thickness in the filled area remained the same. Continuous mass loss was due to the size of unfilled area (holes/cracks) increasing in the surface morphology. Note that we did not measure the film thickness beyond 1500 hr for the AU system due to an increase in the highly degraded unfilled areas.

These results imply that the correlation between film thickness changes and chemical changes follows a linear relationship only in region I (at early stages of the degradation process), but is not well established for the intermediate and later stages of the UV degradation process. In regions II and III, the actual film thickness was greater than the thickness predicted from FTIR results. Using the film thickness as a normalizing factor for analyzing the degradation rates of all FTIR absorbance including the CH band has been an alternative method of quantifying the degradation process.⁶ *Figure 10* shows the relative changes of the C=O band (1726 cm^{-1}), CH band (2960 cm^{-1}), and chain scission (1520 cm^{-1}) normalized by the LSCM measured film thickness at the same exposure time. Results presented in *Figure 10* indicate that the C=O is essentially unchanged with exposure; this is not correct because substantial loss of this species has been observed (see *Figures 3* and *4*).

Chemical and Physical Changes of UV-Exposed AM Coatings

Six replicates of AM coatings were exposed under the same conditions used in the AU system. The upper graph of *Figure 11* shows the chemical changes as a function of three selected FTIR absorbance peaks at 1555 , 1730 , and 2960 cm^{-1} as a function of UV exposure time. The band at 1555 cm^{-1} is related to three different groups: triazine ring, CN attached to the ring, and CH_2 . The band at 1730 cm^{-1} corresponds to the C=O of the acrylic ester group, and the CH band of 2960 cm^{-1} reflects the mass of the coatings. It is clear that the 1555 cm^{-1} band degraded

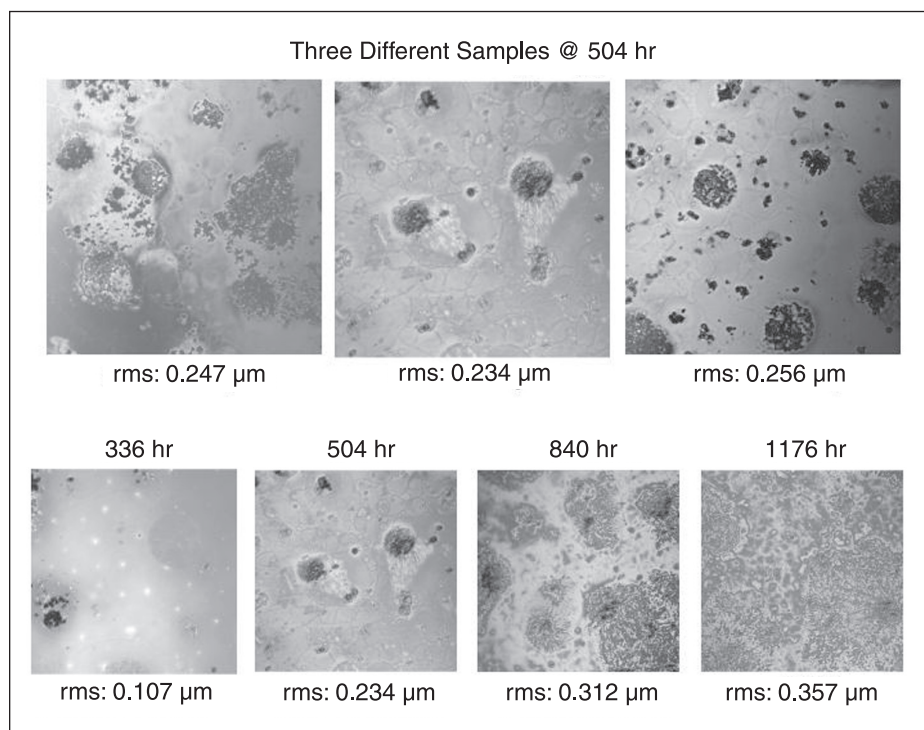


Figure 13—(a) LSCM images of three different AM coatings at the same exposure time (504 hr). (b) Time evolution of surface deformation of an AM coating at four different exposure times. Each LSCM micrograph is $184 \times 184\text{ }\mu\text{m}$ by size.

more rapidly than the 2960 and 1730 cm^{-1} bands, similar to the AU system. The bottom graph of *Figure 11* shows the relative changes of both the 1555 and 1730 cm^{-1} bands normalized by the absorbance of 2960 cm^{-1} at the same exposure time. As in the AU system, the proper parameter for FTIR normalization is not well established.

Figure 12 shows the LSCM film thickness measurements results (upper graph) for AM coatings and the correlation between the “measured” and “predicted” film thickness (bottom graph). In this system, surface degradation occurred so dramatically that the film thickness in the measurable area remained almost the same (the error bars on the thickness measurement were large) after 200 hr of exposure time. Note that the degradation rate of the AM coating was much faster than that of the AU coating. Again by comparing the relative thickness change to predicted change from FTIR (loss in 2960 cm^{-1} band), we conclude that we did not have enough results on the early stages (much earlier than 50 hr) to distinguish the crossover from the early to intermediate stages. The correlation between film thickness and the mass changes measured by FTIR no longer followed a linear relationship, i.e., we have only observed the intermediate and later degradation stages.

Figure 13a shows the surface morphology of three different AM samples after the same exposure time. Although these three samples were cut from the same larger spin-casted specimen, the rate of local degradation/surface deformation is different. The difference in surface morphology at the intermediate/late stages for different samples is noticeable, but it is less noticeable in the thickness and FTIR absorbance measurements. That is, the progress of degradation can be monitored more closely by the surface morphology measurement. In other words, monitoring the local surface deformation can provide insights into the mode of degradation. *Figure 13b* shows the time evaluation of the surface deformation at four different exposure times, starting smooth and featureless at zero exposure time. In addition to some small pits observed to be similar to the exposed AU coatings, there were islands and some underlying network-type microstructures in the immediate stage of the degradation process. These microstructures evolved and surface roughness of the coating increased as observed in the AFM measurements (*Figure 14*).

Note that as far as thickness measurement is concerned, all the thickness values well-represented here were not far from the true (or average) thickness values since the total areas of the pits and surface deformation were still small (less than 20%) and the holes and pits were also shallow. *Figure 15a* illustrates a section of topographic and line profile of an AM coating at 504 hr exposure time, and *Figure 15b* presents the thickness values from 10,000 data points of the measured area. The

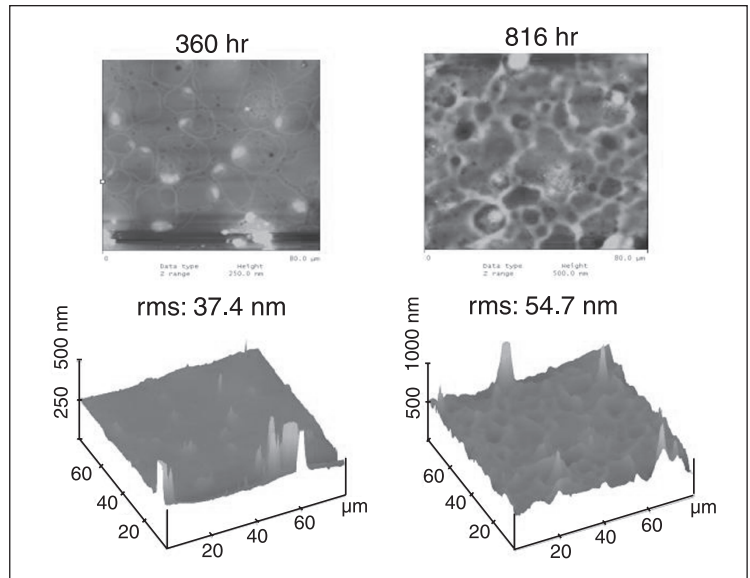


Figure 14—AFM images of AM coatings at two different exposure times.

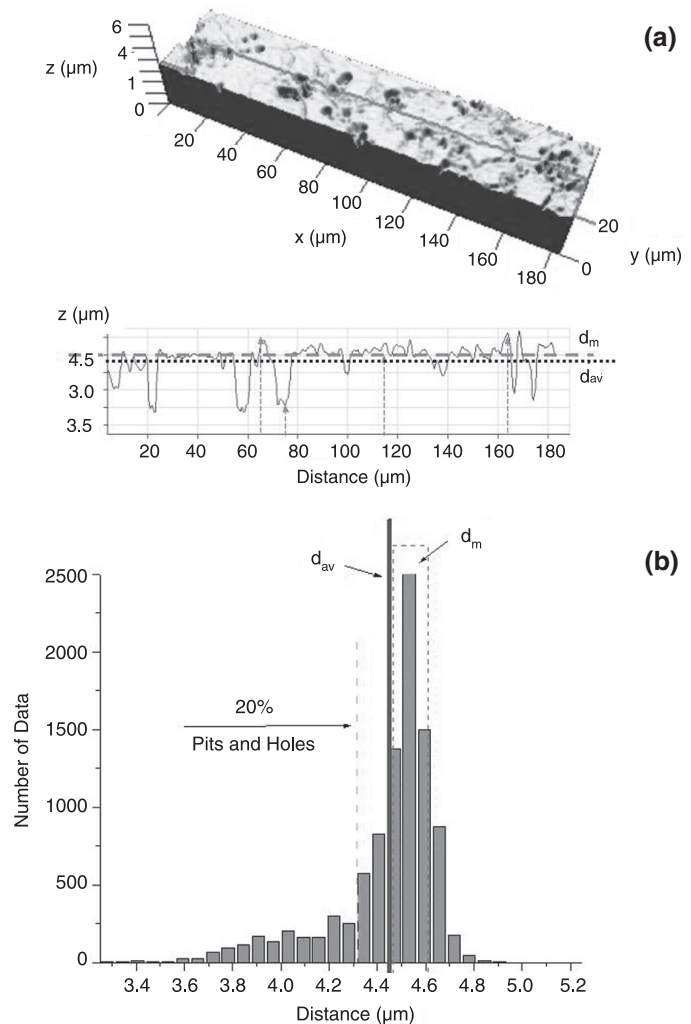


Figure 15—(a) A section of topographic and line profile of an AM coating at 504 hr exposure time, and (b) the statistics of all thickness values from 10,000 data points of the measured area. The value, d_m , is designated as the thickness measured from the filled areas, while the value, d_{av} , is the average thickness of all areas.

thickness value, d_m , obtained from the filled areas was $4.52 \pm 0.08 \mu\text{m}$, and the average thickness, d_{av} , from all the sections including pits and holes was $4.44 \pm 0.05 \mu\text{m}$. With about 20% unfilled areas, the difference between d_m and d_{av} is less than 2%. Moreover, we did not measure the film thickness beyond 1500 hr for the AU system and 840 hr for the AM system when the surface degradation became severe. The discrepancy between the losses in the "measured" thickness to those predicted from the relative loss in CH band was not due to how we measured the thickness. We agree that it will not be correct for just measuring the thickness of the filled areas in the highly degraded surface. In the much later stages, we used the surface roughness/profile to characterize the UV degradation process.

CONCLUDING REMARKS

We have demonstrated the use of laser scanning confocal microscopy as a nondestructive characterization tool for measuring surface morphology and film thickness changes in two coating systems during exposure to UV environments. The relationship between the chemical and physical changes has been investigated. It was found that the mass changes (CH 2960 cm^{-1} band) measured by FTIR only correlated to the film thickness changes measured by LSCM in the early stage of the degradation process. The time frame for pit formation and the onset of the early to intermediate stages of the degradation for the AU system was less than 400 hr, but less than 50 hr for the AM system. More measurements in characterization of pit size and other microstructure as a function of exposure time will be conducted using a combination of AFM and LSCM techniques. Ongoing research also includes: (1) exploring the interfacial heterogeneous hypothesis to investigate the origin and formation of pits and their degradation mechanism, (2) relating the surface roughness to the gloss measurements, and (3) calculating the optical reflectance from measured surface morphology using a ray scattering model. With the continuous efforts in measurements and theoretical modeling, we might be able to establish a "direct" method to investigate the relationship between physical and chemical degradation of coatings exposed to weathering conditions.

References

- (1) Bauer, D.R. and Martin, J.W. (Eds.), *Service Life Prediction of Organic Coatings: A Systems Approach*, ACS Symposium Series, 722, Oxford University Press, 1999.
- (2) Wernstahl, K.M., "Service Life Prediction of Automotive Coatings, Correlating Infrared Measurements and Gloss Retention," *Polym. Degrad. Stab.*, 54, 57 (1996).
- (3) Gerlock, J.L., Smith, C.A., Cooper, V.A., Dubiber, T.G., and Weber, W.H., "On the Use of Fourier Transform Infrared Spectroscopy and Ultraviolet Spectroscopy to Assess the Weathering Performance of Isolated Clearcoats from Different Chemical Families," *Polym. Degrad. Stab.*, 62, 255 (1998).
- (4) Martin, J., Nguyen, T., Byrd, E., Dickens, B., and Embree, N., "Relating Laboratory and Outdoor Exposures of Coatings: I. Cumulative Damage Model and Laboratory Experiment Apparatus," *Polym. Degrad. Stab.*, 75, 193 (2002).
- (5) Nguyen, T., Martin, J., Byrd, E., and Embree, N., "Relating Laboratory and Outdoor Exposures of Coatings: II. Effects of Relative Humidity on Photodegradation of Acrylic Melamine," *JOURNAL OF COATINGS TECHNOLOGY*, 74, No. 932, 31 (2002).
- (6) Croll, S.G. and Skaja, A.D., "Quantitative Spectroscopy to Determine the Effects of Photodegradation on a Model Polyester-Urethane Coatings," *JOURNAL OF COATINGS TECHNOLOGY*, 75, No. 945, 85 (2003).
- (7) Smith, C.A., Gerlock, J.L., Kucherov, A.V., Misovski, T., Seubert, C.M., Carter, R.O. III, and Nichols, M.E., "Evaluation of Accelerated Weathering Tests for Automotive Clears Using Transmission Fourier Transform Infrared Spectroscopy," *Proc. of the FSCT 80th Annual Meeting*, Oct. 30–Nov 1, New Orleans, LA (2002).
- (8) Gerlock, J.L., Peters, C.A., Kucherov, A.V., Misovski, T., Seubert, C.M., Carter, R.O. III, and Nichols, M.E., "Testing Accelerated Weathering Tests for Appropriate Weathering Chemistry: Ozone Filtered Xenon Arc," *JOURNAL OF COATINGS TECHNOLOGY*, 75, No. 936, 35 (2003).
- (9) Osterhold, M. and Glöckner, P., "Influence of Weathering on Physical Properties of Clearcoats," *Prog. Org. Coat.*, 41, 177 (2001).
- (10) Johnson, M.A. and Cote, P.J., "Detrended Fluctuation Analysis of UV Degradation in a Polyurethane Coatings," *JOURNAL OF COATINGS TECHNOLOGY*, 75, No. 941, 51 (2003).
- (11) VanLandingham, M.R., Nguyen, T., Byrd, W.E., and Martin, J.W., "On the Use of the Atomic Force Microscope to Monitor Physical Degradation of Polymeric Coating Surfaces," *JOURNAL OF COATINGS TECHNOLOGY*, 73, No. 923, 43 (2001).
- (12) McKnight, M.E., Marx, E., Nadal, M., Vorburger, T.V., Barnes, P.Y., and Galler, M.A., "Measurements and Predictions of Light Scattering by Clear Epoxy Coatings," *Applied Optics*, 40, No. 13, 2159 (2001).
- (13) Sung, L., Nadal, M.E., McKnight, M.E., Marx, E., and Laurenti, B., "Optical Reflectance of Metallic Coatings: Effect of Aluminum Flake Orientation," *JOURNAL COATINGS TECHNOLOGY*, 74, No. 932, 55 (2002).
- (14) Hunt, F.Y., Marx, E., Meyer, G.W., Vorburger, T.V., Walker, P.A., and Westlund, H.B., "A First Step Towards Photorealistic Rendering of Coated Surfaces and Computer Based Standards of Appearance," in *Service Life Prediction: Methodology and Metrologies*, Martin, J.W. and Bauer, D.R., (Eds.), ACS Symposium Series 805, 437, Oxford University Press, 2002.
- (15) Corle, T.R. and Kino, G.S., *Confocal Scanning Optical Microscopy and Related Imaging Systems*, pp. 37-39, Academic Press, 1996.